

Recovery of Acrylic Acid Using Calcium Peroxide Nanoparticles: Synthesis, Characterisation, Batch Study, Equilibrium, and Kinetics



B. S. De,^a K. L. Wasewar,^{a,*} V. R. Dhongde,^a S. S. Madan,^a and A. V. Gomase^b

^aAdvanced Separation and Analytical Laboratory (ASAL),
Department of Chemical Engineering,
Visvesvaraya National Institute of Technology (VNIT),
Nagpur (M.S) 440010, India

doi: 10.15255/CABEQ.2016.1055b

^bDepartment of Fibres and Textile Processing Technology, Institute
of Chemical Engineering (ICT), Mumbai (M.S) 400019, India

Original scientific paper
Received: December 14, 2016
Accepted: February 6, 2018

Recovery of acrylic acid from aqueous solution using low-cost CaO₂ nanoparticles was investigated. CaO₂ nanoparticles were synthesized by co-precipitation technique and characterised using XRD and FTIR. A mechanism was proposed for adsorption of acrylic acid onto CaO₂ nanoparticles based on FTIR analysis. Acrylic acid recovery is highly dependent on contact time, CaO₂ nanoparticle dosage, initial acrylic concentration, and temperature. Langmuir, Freundlich, Dubinin-Radushkevich, Tempkin, Hill, Redlich-Peterson, Sips and Toth isotherms were used and well represented by Redlich-Peterson isotherm ($R^2 = 0.9998$) as compared to other isotherms. Kinetic studies revealed pseudo-second-order kinetics ($k_2 = 1.962 \cdot 10^{-4} \text{ g mg}^{-1} \text{ min}^{-1}$) for adsorption of acrylic acid onto CaO₂ nanoparticles. CaO₂ nanoparticles exhibited high acrylic acid recovery over varied concentration ranges. The acrylic acid can be regenerated by desorption from the surface of adsorbent and utilised for numerous applications. The presented results may be useful for the design of adsorption system using nanoparticles, which can be extended to other systems.

Keywords:

acrylic acid, adsorption, calcium peroxide nanoparticles, equilibrium, kinetics, batch study

Introduction

Acrylic acid or vinyl formic acid (CH₂=CH-COOH) is an important organic acid for the manufacture of polymeric flocculants for water treatment, intermediates in the preparation of super-absorbent materials, adhesives and sealants, surface coatings, polishes, surfactants, plastic additives, dispersants, and textiles.¹ The global market for acrylic acid is estimated to reach US\$ 20 billion in 2018, and its demand to reach 260 KTPA by 2020.² The partial oxidation of propene, a single-step process, is the most commercial method for the production of acrylic acid, but the yield is at most (50 – 60 %), causing large amounts of waste. The two-step process achieves an overall yield of 90 % via acrolein.³

Several biotechnological processes for the production of acrylic acid have been developed, which provide an attractive alternative, but the high cost of the recovery step in the generation of the acid poses a major challenge in its commercialization.⁴ Conse-

quently, it is essential to develop a simple and cost-effective method for the recovery of acrylic acid. Many studies have been conducted in respect of recovery of carboxylic acids from waste stream/dilute solution. Hybrid and intensified separation processes, such as reactive distillation, extractive distillation, pervaporation and reactive distillation have been proven to be effective for the recovery of carboxylic acids.^{5–9} Adsorption has been proven to be an efficient technique to remove various compounds.^{10–26} Also, carboxylic acids can be recovered by adsorption.^{27–36} The literature on the removal of a few carboxylic acids from aqueous solutions by adsorption is summarised in Table 1, but limited work on the adsorption of acrylic acid from aqueous streams is available.

The selection of proper adsorbent having sufficient selectivity and capacity is the key to successful recovery/removal. A large specific area is of great significance for the adsorbents, which is attained by manufacturing techniques that result in solids with a microporous structure. Consequently, researchers have a growing interest to develop a novel cost-effective adsorbent with high adsorptive

*Corresponding author: k_wasewar@rediffmail.com;
klwasewar@che.vnit.ac.in; dr.kailaswasewar@gmail.com

Table 1 – Summary of a few studies conducted on carboxylic acid adsorption

Carboxylic acid	Adsorbent	Type of study
Oxalic acid, malonic acid, succinic acid, gallic acid, EDTA, TTHA ³⁰	Titanium dioxide	Kinetic
Acetic acid, propionic acid, butyric acid ³¹	Activated carbon from watermelon shells	Equilibrium
Formic acid, acetic acid, propionic acid ³²	α -Al ₂ O ₃	Kinetic
Acetic, citric, lactic, and tartaric acids ²⁷	Hydrogels	Equilibrium
Glycolic acid and acetic acid ²⁸	AmberliteIRA-67	Equilibrium
α -Toluic acid ²⁹	CaO ₂ nanoparticles	Equilibrium, kinetic thermo-dynamic

capacity. Nanotechnology offers new promises in recent years. Nanoparticles possess distinct physical and chemical properties, and they may exhibit totally new characteristics as compared to their bulk form due to their high surface-to-volume ratio, and because of their small size, quantum effects come into play.³⁷

Calcium peroxide (CaO₂) has proven its effectiveness in enhanced bioremediation of BTEX (benzene, toluene, ethylbenzene and xylene) contaminated soil³⁸ and its use has also increased the remediation of soil.³⁹ It has been used to provide oxygen for contaminant biodegradation in saturated soil, but studies have revealed that rate of oxidation reaction between calcium peroxide and contaminant is extremely slow.⁴⁰ Therefore, to overcome this problem, nanosized CaO₂ can be used, which can increase the surface-to-volume ratio and the rate of reaction.

In this study, the candidacy of synthesised CaO₂ nanoparticles as an effective adsorbent for the recovery of acrylic acid from the aqueous stream has been studied. The effect of contact time, initial concentration, adsorbent dosage, and temperature on adsorption capacity was investigated by conducting batch experiments. Consequently, equilibrium isotherm and kinetics were also evaluated to design a batch adsorption system for the recovery of acrylic acid from aqueous stream.

Materials and methods

Reagents

Polyethylene glycol (PEG 200), ammonia solution (NH₃·H₂O, 25 %), calcium chloride (CaCl₂, 99.5 %), hydrogen peroxide (H₂O₂, 35 %), sodium

hydroxide (NaOH) were supplied by Merck (India) and used without further treatment or purification. Acrylic acid (99 %) was obtained from S D Fine-Chem Ltd. The stock solutions of acrylic acid (7206 mg L⁻¹) were prepared fresh every week by dilution of 7±0.1 mL of acrylic acid with double distilled water, and to obtain working solutions of varying concentrations for further experiments.

Preparation of CaO₂ nanoparticles

CaO₂ nanoparticles were synthesised using a slightly modified co-precipitation technique.^{41,42} In the present case, six grams of CaCl₂ was dissolved in 60 mL distilled water along with 30 mL ammonia solution (1 M) and 240 mL PEG 200 in a 1000-mL beaker. PEG 200 was used as a surface modifier, which is important for obtaining nanoparticles as it provides steric stabilization by the formation of micelles. The solution was stirred at a constant rate with the continuous addition of 30 mL H₂O₂ (30 %) at a rate of three drops per minute. A clear and colourless to yellowish solution was obtained after 3 hours of stirring. To precipitate the product, NaOH solution (pH 13) was added slowly until pH 11.5 was obtained and the mixture changed to a white suspension. The precipitate was separated by centrifugation at 10000 RPM and the white powder obtained was washed three times with 0.1 M NaOH solution, followed by washing with distilled water until pH of 8.4 for the residue water was achieved. The obtained precipitate was then dried in an evacuated oven for 2 hours at 353.15 K to obtain CaO₂ nanoparticles. A vacuum oven was used to avoid contamination and prevent excess oxygen from coming in contact while drying, which may result in formation of CaO instead of CaO₂. A vacuum oven also allows drying of nanoparticles at much lower temperature. A schematic representation of the process is presented in Fig. 1. The reactions involved in the synthesis of CaO₂ nanoparticles by co-precipitation method are:



Batch adsorption studies

Adsorption experiments were conducted to study the effect of initial concentration of acrylic acid (720–7206 mg L⁻¹), contact time (5–200 min), adsorbent dosage (0.01–0.1 g per 10 mL), and temperature (300.15 – 313.15 K) on the removal efficiency of acrylic acid. The experiments were carried out by taking 10 mL of acrylic acid of known concentration in a 100-mL Erlenmeyer flask with a known adsorbent dosage. Orbital shaking incubator

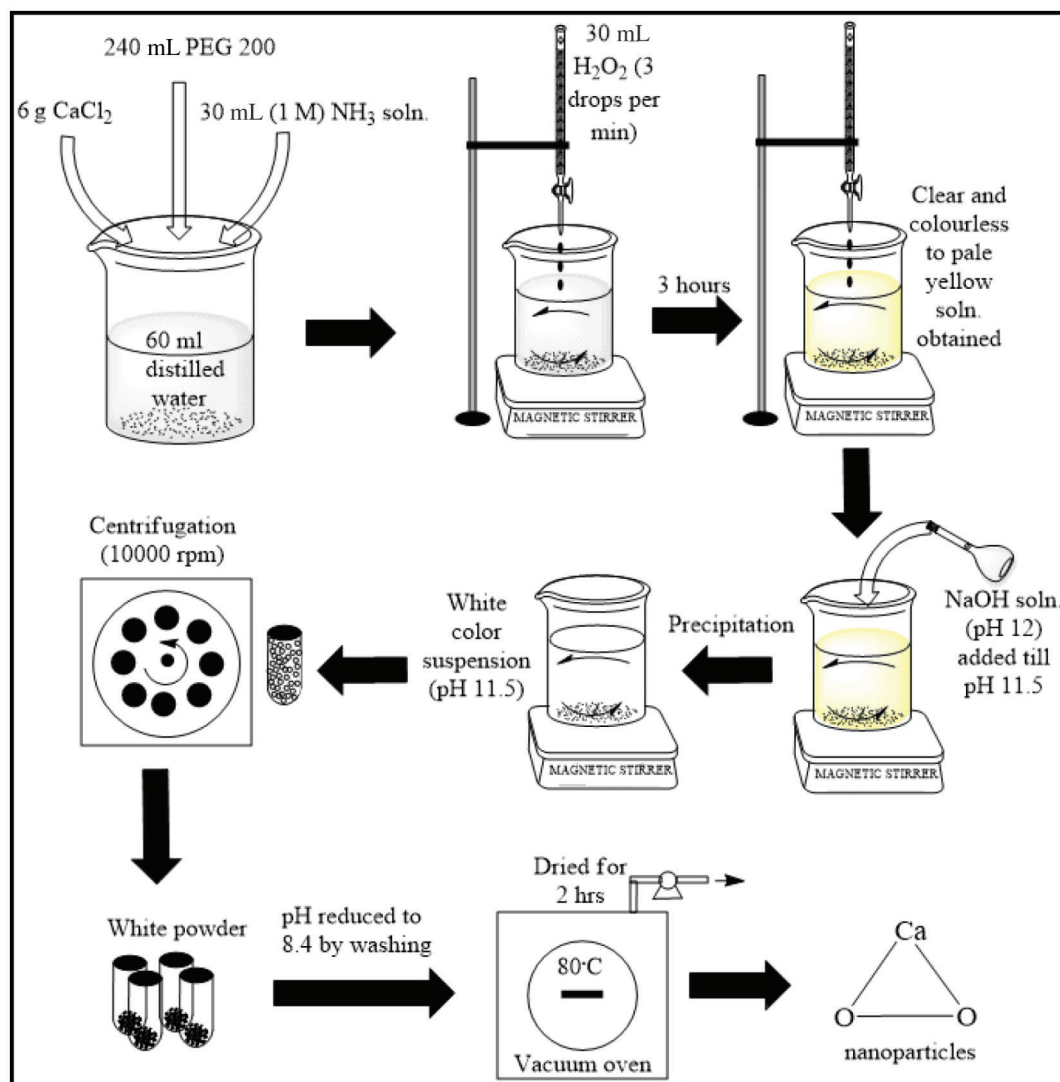


Fig. 1 – Schematic representation of the synthesis of CaO_2 nanoparticles using co-precipitation technique

(REMI S-24BL, India) was employed to shake the mixture for a minimum of 200 minutes, and the samples were centrifuged at 3000 rpm for 5 minutes after shaking to separate the spent CaO_2 nanoparticles. The aqueous concentration of acrylic acid in the supernatant was determined by titration with NaOH (0.01 M) and phenolphthalein as an indicator. A fresh NaOH solution was prepared for each set of experiments. The concentration range of acrylic acid used in the study is based on highest concentration of acrylic acid that can be found in any aqueous stream. A few experiments were repeated and analysed, the consistency was observed within $\pm 2\%$. The pH was measured by a digital pH meter (Spectral Lab Instrumental Pvt. Ltd. India) which was calibrated with three buffers (pH 4.0, 7.0 and 10.0) daily.

The removal efficiency, E (%), of acrylic acid was calculated as a ratio between acrylic acid adsorbed at time t , to its initial aqueous concentration as:

$$E(\%) = \frac{C_0 - C_t}{C_0} \cdot 100 \quad (3)$$

where, C_0 (mg L^{-1}) is the initial aqueous acrylic acid concentration, and C_t (mg L^{-1}) is the aqueous acrylic acid concentration at time t (min).

The amount of acrylic acid adsorbed (q_t , mg g^{-1}) onto CaO_2 nanoparticles at time t was determined as:

$$q_t = \frac{(C_0 - C_t) \cdot V}{m} \quad (4)$$

where, m (g) is mass of adsorbent, and V (L) is the volume of aqueous solution. The amount of acrylic acid adsorbed onto CaO_2 nanoparticles at equilibrium q_e is equal to q_p , while C_t was addressed as C_e at equilibrium time. A trial run was performed using conventional CaO_2 at the start of experiment. The conventional CaO_2 was observed to form lumps during adsorption, and the particles were not well

dispersed even at longer shaking time. This lead to a low adsorption efficiency with the use of conventional CaO_2 . Also, a high dosage of CaO_2 was required for effective acrylic acid recovery due to particle aggregation and large particle size.

Desorption study

A point study on desorption of acrylic acid from CaO_2 nanoparticles was performed for the sample that showed highest level of adsorption. An ultrasonicator water bath (LABMAN LMUC-4) was employed for this purpose. 0.1 g spent CaO_2 nanoparticles in 10 mL distilled water was taken in an Erlenmeyer flask at 333.15 K. The sample was sonicated for 30 minutes and the aliquot of the resulting solution analysed by titration to determine the amount of desorbed acrylic acid.

Results and discussion

Characterisation of CaO_2 nanoparticles

X-ray diffraction (XRD) analysis of CaO_2 nanoparticles was carried out by X-ray diffractometer (PAN analytical X'pert PRO) in the 2θ range from 10° to 100° with a step size of 0.01° using a Cu X-ray tube ($\lambda = 0.15406$ nm) to ascertain the chemical composition (Fig. 2). The five dominant peaks of the XRD spectra at 2θ values of 29.68, 36.19, 47.74, and 60.85 are in agreement with XRD of CaO_2 (JCPDS – 00 – 003-0865). The comparison of 2θ and d -spacing values of the standard CaO_2 with the synthesised CaO_2 nanoparticles are listed in Table 2, and the analogy confirms its chemical composition. The Debye-Scherrer equation was used to determine the average particle size of CaO_2 nanoparticles from the XRD peak (110) pattern using the following expression:

$$D = \frac{k\lambda}{\beta \cos \theta} \quad (5)$$

Table 2 – Comparison of 2θ and d -spacing values of the standard CaO_2 with the synthesised CaO_2 nanoparticles

Sr. No.	CaO ₂ (JCPDS – 00-003-0865)			Synthesised CaO ₂ nanoparticles	
	2θ (degree)	d-spacing (Å)	Miller indices (h k l)	2θ (degree)	d-spacing (Å)
1	30.27	2.95	0 0 2	30.96	2.88
2	35.59	2.52	1 1 0	35.74	2.50
3	47.30	1.92	1 1 2	47.32	1.91
4	51.59	1.77	2 0 0	51.00	1.78
5	53.21	1.72	1 1 3	53.42	1.71

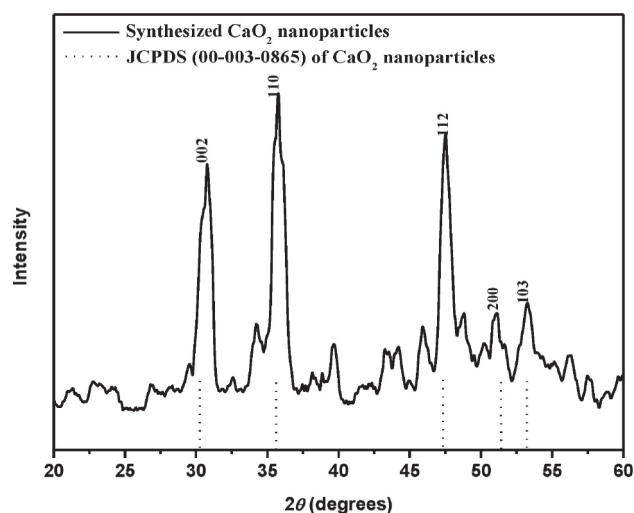


Fig. 2 – X-Ray diffraction pattern of synthesised CaO_2 nanoparticles and standard JCPDS (000-03-0865) of CaO_2 (dotted line)

where k is the Debye-Scherrer constant ($k = 0.9$), λ is the wavelength of the incident X-ray radiation ($\lambda = 0.15406$ nm), θ is the Bragg's angle in radians, and β is the full width at half maximum (FWHM) of the most intense peak (002). The calculated size of the nanocrystallite was found to be 29.38 nm.

The Fourier Transfer Infrared (FTIR) spectrum of CaO_2 nanoparticles, pure acrylic acid, and acrylic acid adsorbed onto CaO_2 nanoparticles were obtained using Shimadzu Corporation IRAffinity-1 (Japan) apparatus within the range 4000 to 400 cm^{-1} . Fig. 3 represents the plot of percent transmission versus wave number that was measured from FTIR. The spectra were analysed for different types of functional groups for the further confirmation of CaO_2 nanoparticles and adsorption of acrylic acid onto CaO_2 nanoparticles, thus suggesting a suitable mechanism for the adsorption process. The band positions present at 748 and 711 cm^{-1} correspond to O–O stretch, and that of 560 and 508 cm^{-1} correspond to O–Ca–O stretch⁴³ for CaO_2 nanoparticles (Fig. 3(a)). The spectrum of pure acrylic acid (Fig. 3(b)) shows a band at 1704 cm^{-1} which refers to C=O stretch,⁴⁴ followed by bands at 1635 , 1243 , 1048 , 985 , 925 , 820 , and 650 cm^{-1} which correspond to C=C stretch, CH in-plane bend, CH_2 rocking, out of phase CH_2 wag, and out-of-plane CH bend, out-of-plane OH bend, CH_2 twist, and CO_2 in-plane bend, respectively.⁴¹ The band that corresponds to C=O stretch in the spectrum of pure acrylic acid is low in the spectrum of acrylic acid adsorbed onto CaO_2 nanoparticles (Fig. 3(c)), which advocates the fact that COO group is chemically attached on the surface of CaO_2 nanoparticles, thus proving the adsorption of acrylic acid onto CaO_2 nanoparticles surface. It was also observed from the

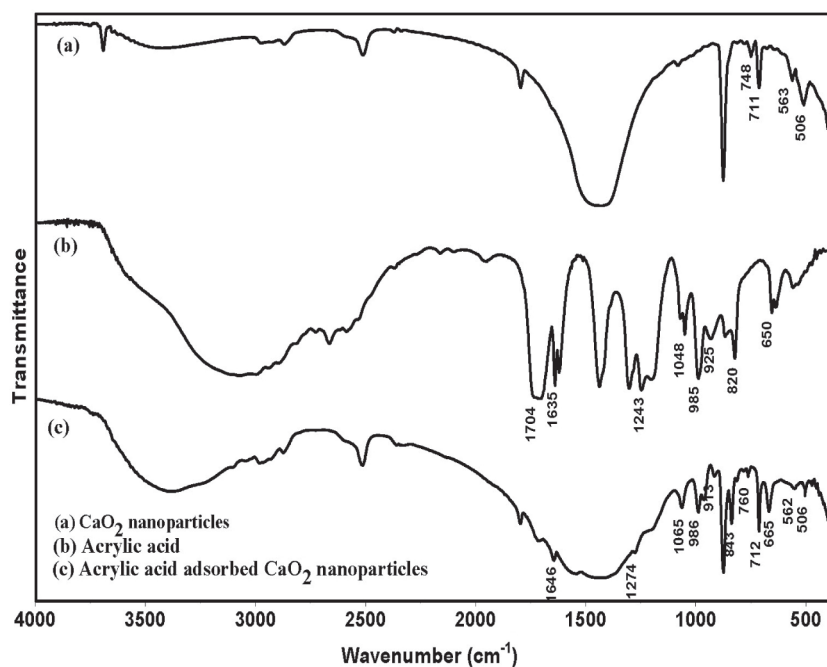


Fig. 3 – FTIR spectrum of (a) CaO_2 nanoparticles, (b) acrylic acid, and (c) acrylic acid adsorbed CaO_2 nanoparticles

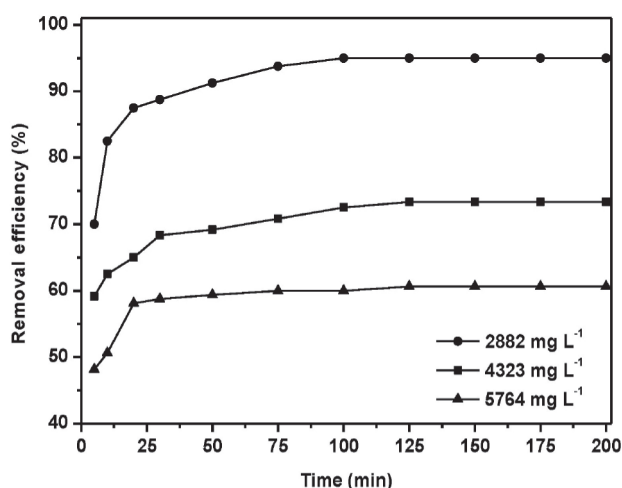


Fig. 4 – Effect of contact time on the removal efficiency of acrylic acid onto CaO_2 nanoparticle (initial acrylic acid concentration = 2882, 4323, 5764 mg L^{-1} , adsorbent dosage = 1 g L^{-1} , temperature = 300.15 K)

spectrum of acrylic acid adsorbed onto CaO_2 nanoparticles (Fig. 3(c)), that the bands at 1635, 1243, 1048, 985, 925, 820, and 650 cm^{-1} that correspond to the acrylic acid spectrum (Fig. 3(b)), were shifted to 1646, 1274, 1065, 986, 913, 843, and 665 cm^{-1} , respectively, after adsorption. Also, the bands at 760, 712, 560, and 506 cm^{-1} , in the case of acrylic acid adsorbed CaO_2 nanoparticles, match the bands of CaO_2 nanoparticles, signifying that the basic characteristics of CaO_2 nanoparticles were retained even after the adsorption of acrylic acid.

Thus, it can be concluded from the comparison of FTIR spectra that acrylic acid adsorbs chemically onto the surface of CaO_2 nanoparticles.

Effect of contact time

To investigate the effect of contact time on removal efficiency, experiments were conducted by varying the contact time from 5–200 minutes to ensure equilibrium for three different acrylic acid concentrations (2882, 4323, and 5764 mg L^{-1}) with constant adsorbent dosage (1 g L^{-1}) and temperature (300.15 \pm 1 K). The time required to reach equilibrium occurred relatively earlier in solutions containing lower acrylic acid concentrations than in those containing higher concentrations, which may be due to saturation of active sites available for adsorption (Fig. 4). The higher initial concentration of acrylic acid enhances the adsorption process and the increased adsorptive capacity of CaO_2 nanoparticles due to higher concentration gradient. The initial rate of adsorption onto CaO_2 nanoparticles was very fast, which corresponds to external surface adsorption, followed by the gradual adsorption stage, whose contribution to the total acrylic acid adsorption was relatively small. Finally, equilibrium was established within 125 minutes and was slightly dependent on initial acrylic acid concentration and considered as the optimum contact time for further studies.

Effect of CaO_2 nanoparticles dosage

The effect of adsorbent dosage (1–10 g L^{-1}) on the removal efficiency was investigated at constant temperature (300.15 \pm 1 K) and contact time (125 min) with initial acrylic acid concentration 4323 mg L^{-1} . Fig. 5 reveals that the removal efficiency increased with an increase in adsorbent dosage. It is certainly due to more active sites for the adsorption of acrylic acid from an increased amount of CaO_2 nanoparticles. A seventy-five percent removal efficiency for 1 g L^{-1} CaO_2 nanoparticles was observed, which enhanced with an increase in adsorbent dosage up to 99 % (7 g L^{-1} adsorbent dosage). On further increase in adsorbent dosage, the increase in removal efficiency was not considerable. Thus, the optimum CaO_2 nanoparticles dosage was found to be 7 g L^{-1} . However, due to the limited amount of nanoparticles available, further studies were conducted at 1 g L^{-1} adsorbent dosage.

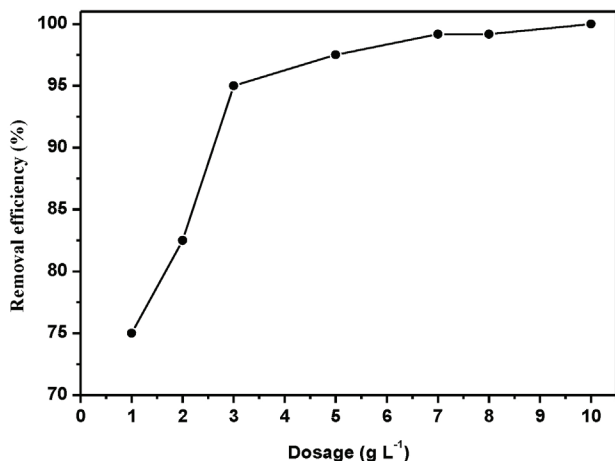


Fig. 5 – Effect of adsorbent dosage on the removal efficiency of acrylic acid onto CaO_2 nanoparticles (initial acrylic acid concentration = 4323 mg L^{-1} , temperature = 300.15 K , time = 125 min)

Effect of initial acrylic acid concentration

The removal efficiency is dependent on the initial acrylic acid concentration as it serves as a principle driving force to overcome all mass transfer resistances of the acrylic acid between aqueous and solid phase. This was studied by varying the acrylic acid concentration at the constant adsorbent dosage (1 g L^{-1}), contact time (125 min), and temperature ($300.15 \pm 1 \text{ K}$), as depicted in Fig. 6. As the initial acrylic acid concentration increased from 720 to 7206 mg L^{-1} , the removal efficiency gradually reduced from 99.9 to 50% until equilibrium was reached. This was almost certainly because of the saturation of available sites for adsorption. However, the adsorption efficiency for the concentrations 1500 mg L^{-1} and 3000 mg L^{-1} was observed to be almost the same. This may be attributed to the fact that the difference in concentration was not high enough to bring about a noticeable removal efficiency in this concentration range.

Effect of temperature

The adsorption of acrylic acid was studied at different temperatures (300.15 to 313.15 K) using CaO_2 nanoparticles as an adsorbent with initial acrylic acid concentration 2882 , 4323 , and 5764 mg L^{-1} . A decrease in removal efficiency with the increase in the solution temperature was observed (Fig. 7), which was attributed to an exothermic adsorption process. This trend could be attributed to the weakening of adsorptive forces between active sites of CaO_2 nanoparticles and acrylic acid, as well as between the adjacent molecules of the adsorbed phases. The optimum adsorption temperature of acrylic acid with CaO_2 nanoparticles was observed at 300.15 K , which will have the benefit of operation at ambient temperature.

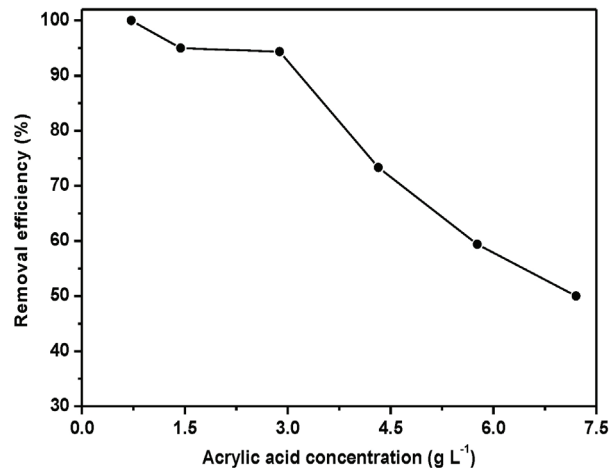


Fig. 6 – Effect of initial concentration on the removal efficiency of acrylic acid onto CaO_2 nanoparticles (adsorbent dosage = 1 g L^{-1} , temperature = 300.15 K , time = 125 min)

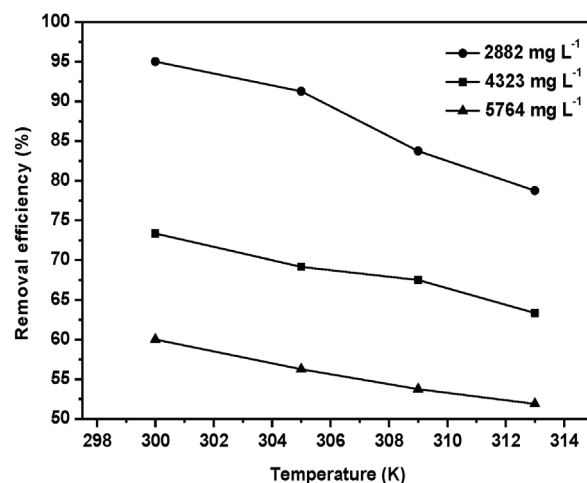


Fig. 7 – Effect of temperature on the removal efficiency of acrylic acid onto CaO_2 nanoparticles (initial acrylic acid concentration = 2882 , 4323 , 5764 mg L^{-1} , adsorbent dosage = 1 g L^{-1} , time = 125 min , temperature = $300.15 - 313.15 \text{ K}$)

Recovery of acrylic acid after desorption

The desorption of acrylic acid from the surface of CaO_2 nanoparticles was performed to check the economic feasibility. The point study revealed percent desorption of acrylic acid to be 62.4% . During sonication, ultrasonic waves generate vibrations in adsorbent and adsorbate, provoking desorption of the most weakly bound molecules, such as those adsorbed by physic-sorption. However, since most of the acrylic acid is adsorbed by chemisorption, the vibration does not have sufficient energy to break the acid-adsorbent bonds on the surface of CaO_2 nanoparticles.

Adsorption isotherms

In order to describe how acrylic acid molecules will interact with CaO_2 nanoparticles, providing a

panorama of the course taken by the system under study in a concise form, and to optimize the design of an adsorption system to remove acrylic acid from aqueous solution, proper knowledge of adsorption properties and equilibrium data, i.e., adsorption isotherms, is required. To optimize the design of the adsorption system, it is essential to establish the most appropriate correlation for the equilibrium curve. Adsorption equilibrium is established when the amount of acrylic acid adsorbed onto CaO₂ nanoparticles in unit time is equal to the amount be-

ing desorbed. The equilibrium acrylic acid concentration remains constant, and plotting solid phase concentration against liquid phase concentration graphically depicts the equilibrium adsorption isotherm.

In this study, various two-and three-parameter models, such as Langmuir, Freundlich, Dubinin-Radushkevich, Temkin, Hill, Redlich-Peterson, Sips and Toth models (Table 3) were fitted in their non-linear form to estimate the model parameters. Langmuir isotherm assumes monolayer adsorption,

Table 3 – Expressions of non-linear adsorption isotherm models and the different parameters involved

Isotherm	Non-linear form	Adjustable model parameters and R^2
Langmuir ⁴⁵	$q_e = \frac{Q_0 b C_e}{1 + b C_e}$ Q_0 – maximum monolayer coverage capacities (mg g ⁻¹) b – Langmuir isotherm constant (dm ³ mg)	Q_0 (mg g ⁻¹) = 3620 b (dm ³ mg) = 0.008171 $R^2 = 0.9931$
Freundlich ⁴⁶	$q_e = K_F f C_e^{1/n}$ K_F – Freundlich isotherm constant (mg g ⁻¹) (dm ³ g ⁻¹) ^{n} related to adsorption capacity n – adsorption intensity	K_F (mg g ⁻¹) (dm ³ g ⁻¹) ^{n} = 568.1 $n = 4.33$ $R^2 = 0.96$
Dubinin-Radushkevich ⁴⁷	$q_e = q_s \exp\left(\frac{(RT \ln(1 + 1/C_e))^2}{-2E^2}\right)$ q_s – theoretical isotherm saturation capacity (mg g ⁻¹) E – energy of adsorption (kJ mol ⁻¹)	q_s (mg g ⁻¹) = 3405 E (kJ mol ⁻¹) = 23.17 $R^2 = 0.9719$
Temkin ⁴⁸	$q_e = \frac{RT}{b_T} \ln A_T C_e$ A_T – Temkin isotherm equilibrium binding constant (L g ⁻¹) b_T – Temkin isotherm constant	A_T (L g ⁻¹) = 0.1556 $b_T = 3.894$ $R^2 = 0.9904$
Hill ⁴⁹	$q_e = \frac{q_{s_H} C_e^{n_H}}{K_D + C_e^{n_H}}$ q_{s_H} – Hill isotherm maximum uptake saturation (mg L ⁻¹) n_H – Hill cooperativity coefficient of the binding interaction	q_{s_H} (mg L ⁻¹) = 4027 $n_H = 0.7048$ $R^2 = 0.9996$
Redlich-Peterson ⁵⁰	$q_e = \frac{K_R C_e}{1 + a_R C_e^g}$ K_R – Redlich-Peterson isotherm constant (L g ⁻¹) a_R – Redlich-Peterson isotherm constant (mg ⁻¹) g – Redlich-Peterson isotherm exponent	K_R (L g ⁻¹) = 36.87 a_R (mg ⁻¹) = 0.01745 $g = 0.9318$ $R^2 = 0.9998$
Sips ⁵¹	$q_e = \frac{K_S C_e^{\beta_S}}{1 + a_S C_e^{\beta_S}}$ K_S – Sips isotherm model constant (L g ⁻¹) a_S – Sips isotherm model constant (L mg ⁻¹) β_S – Sips isotherm model exponent	K_S (L g ⁻¹) = 101.9 a_S (L mg ⁻¹) = 0.0253 $\beta_S = 0.7048$ $R^2 = 0.9996$
Toth ⁵⁰	$q_e = \frac{q_{S_{Th}} C_e}{(K_{Th} + C_e^{Th})^{1/Th}}$ $q_{S_{Th}}$ – Toth theoretical isotherm saturation capacity (mg g ⁻¹) K_{Th} – Toth isotherm model constant (L g ⁻¹) Th – Toth isotherm model exponent	$q_{S_{Th}}$ (mg g ⁻¹) = 4107 K_{Th} (L g ⁻¹) = 13.43 $Th = 0.6155$ $R^2 = 0.9996$

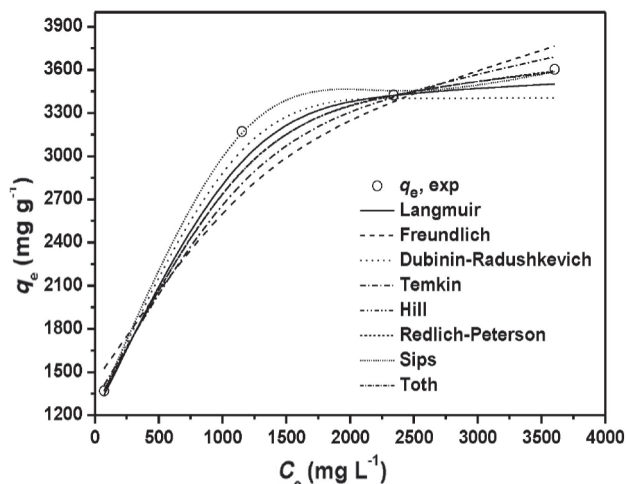


Fig. 8 – Comparisons of various non-linear two- and three-parameter adsorption isotherm models used in the study (initial acrylic acid concentration = 4323 mg L⁻¹, adsorbent dosage = 1 g L⁻¹, time = 125 min, and temperature = 300.15 K)

i.e., the adsorbed layer is one molecular in thickness, and with a finite number of identical sites onto a homogeneous surface.⁴⁵ Freundlich isotherm model describes the non-ideal and reversible adsorption and can be applied to multilayer adsorption with non-uniform distribution of adsorption sites and affinities over the heterogeneous surface.⁴⁶ Dubinin-Radushkevich isotherm was conceived to express the adsorption mechanism with Gaussian energy distribution onto a heterogeneous surface.⁴⁷ Temkin isotherm model takes into account adsorbent-adsorbate interactions and assumes that the heat of adsorption of all molecules in the layer would decrease linearly with coverage by ignoring the extremely low and high values of concentrations.⁴⁸ Hill isotherm assumes adsorption to be a cooperative phenomenon to describe the binding of different species onto homogeneous substrate.⁴⁹ Redlich-Peterson isotherm is a hybrid of both Langmuir and Freundlich isotherms and is used to represent adsorption equilibria over a wide concentration range, and can be applied either to the homogeneous or heterogeneous system.⁵⁰ Sips isotherm model is also a combination of Langmuir and Freundlich's expressions deduced for predicting the heterogeneous adsorption system and overcoming the limitation of increasing adsorbate concentration associated with Freundlich isotherm model.⁵¹ Toth isotherm model was developed to improve Langmuir isotherm and is useful in describing a heterogeneous adsorption system satisfying both low and high-end boundary of the concentration.⁵⁰ The non-linear regression was performed to obtain the best fit for the models.

To test the best fitting isotherm to the experimental data, the coefficient of determination, R^2 ,

was used, and all the parameters and R^2 values are presented in Table 3. Fig. 8 shows the experimental and predicted two- and three-parameter isotherms by a non-linear method for the adsorption of acrylic acid onto CaO₂ nanoparticles. The Langmuir, Temkin, and Hill isotherms have almost the same high values of R^2 as compared to Freundlich and Dubinin-Radushkevich for the two-parameter isotherm. Here, the Langmuir isotherm indicates that uptake occurs on a homogeneous surface by monolayer adsorption and chemisorption behaviour due to the formation of an ionic or covalent bond between adsorbent and adsorbate. Additionally, the values of n for Freundlich isotherm are within the range of 1–10, suggesting that the acrylic acid could be readily adsorbed onto CaO₂ nanoparticles, and that the adsorption was beneficial for acrylic acid. The three-parameter isotherm models give high values of R^2 . The Sips and Toth isotherms have the same values of R^2 . The highest R^2 value for Redlich-Peterson isotherm suggests the best curve model of given experimental data; since its parameter g is close to one, it is in accordance with the low concentration limit of Langmuir isotherm model. The isotherm models fitted the experimental data in the order of Redlich-Peterson > Sips, Toth and Hill > Langmuir > Temkin > Dubinin-Radushkevich > Freundlich.

Adsorption kinetics

Adsorption kinetics describes the rate of adsorption and the solute uptake rate, which in turn controls the residence time and hence the size of adsorption equipment. In order to deduce the adsorption mechanism of acrylic acid onto CaO₂ nanoparticles, pseudo-first-order and pseudo-second-order models were used for three different acrylic acid concentrations (2882, 4323, and 5764 mg L⁻¹) at the temperature of 300.15 K. Pseudo-first-order model explains the adsorption between solid and liquid system based on the physisorption capacity of the solid, and pseudo-second-order model usually describes the experimental data for the chemisorption case.²⁹ The non-linear forms of the two models are summarised in Table 4, which were solved using a non-linear regression technique.

The pseudo-first-order and pseudo-second-order kinetic models were fitted to the experimental data (Fig. 9 and Fig. 10) to predict the adsorption kinetics of acrylic acid onto CaO₂ nanoparticles. The pseudo-first-order rate constant k_1 , pseudo-second-order rate constant k_2 , experimental equilibrium adsorption capacities $q_{e,exp}$, calculated equilibrium adsorption capacities $q_{e,cal}$ and the coefficient of determination R^2 are all given in Table 5. The $q_{e,cal}$ values calculated from pseudo-first-order kinetic mod-

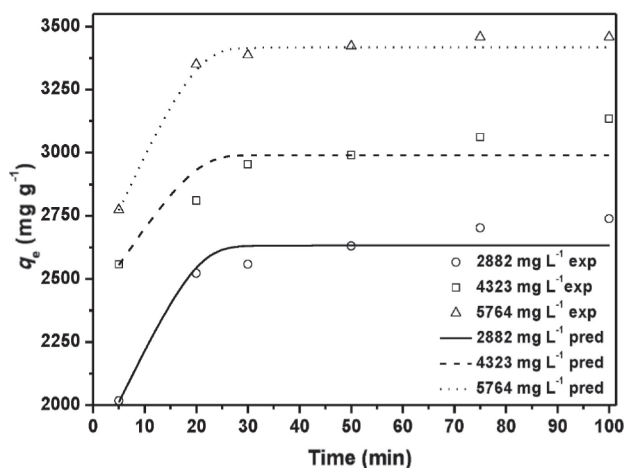


Fig. 9 – Pseudo-first-order kinetic fit for adsorption of acrylic acid onto CaO_2 nanoparticles (initial acrylic acid concentration = 2882, 4323, 5764 mg L^{-1} , adsorbent dosage = 1 g L^{-1} , time = 125 min, and temperature = 300.15 K)

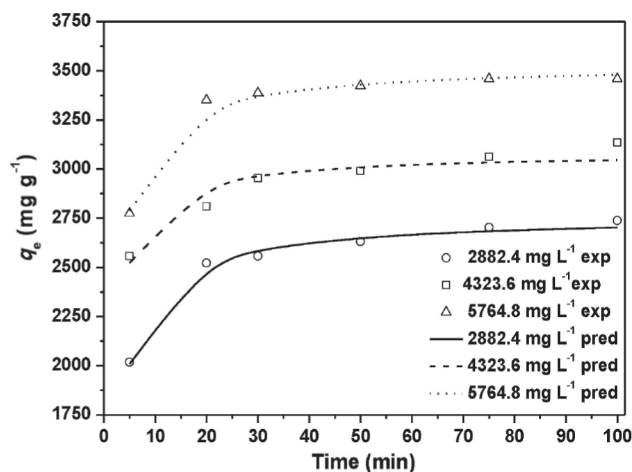


Fig. 10 – Pseudo-second-order kinetic fit for adsorption of acrylic acid onto CaO_2 nanoparticles (initial acrylic acid concentration = 2882, 4323, 5764 mg L^{-1} , adsorbent dosage = 1 g L^{-1} , time = 125 min, and temperature = 300.15 K)

Table 4 – Non-linear forms of kinetic models used in the present study for the adsorption of acrylic acid onto CaO_2 nanoparticles

Model	Non-linear form	Plot	Parameters
Pseudo-first-order	$q_t = q_e (1 - \exp^{-k_1 t})$ q_t – amount of adsorbate at time t (mg g^{-1}) q_e – equilibrium adsorption capacity (mg g^{-1}) k_1 – rate constant of pseudo-first-order kinetics (min^{-1}) t – time (min)	q_t vs. t	k_1, q_e
Pseudo-second-order	$q_t = \frac{k_2 q_e^2 t}{1 + k_2 q_e t}$ k_2 – rate constant of pseudo-second-order kinetics ($\text{mg mg}^{-1} \text{min}^{-1}$) $h = k_2 q_e^2$ h – initial adsorption rate ($\text{mg mg}^{-1} \text{min}^{-1}$)	q_t vs. t	k_2, q_e, h

el differed appreciably from the experimental values $q_{e,\text{exp}}$, but the $q_{e,\text{cal}}$ values calculated from the pseudo-second-order kinetic model are very close to $q_{e,\text{exp}}$ values. Moreover, on comparing the values of R^2 , pseudo-second-order kinetic model yielded better results as compared to pseudo-first-order as the values are much closer to unity. Therefore, the adsorption data were well represented by pseudo-second-order kinetics, suggesting that the rate-limiting step of acrylic acid adsorption onto CaO_2 nanoparticles is controlled by chemisorption behaviour.⁵²

Conclusions

The characteristics and mechanism of acrylic acid adsorption onto CaO_2 nanoparticles is reported in the present study. CaO_2 nanoparticles were synthesised and characterised using XRD and FTIR to confirm its formation. The batch adsorption test revealed that the recovery of acrylic acid increased with contact time and adsorbent dosage, and decreased with increase in initial acrylic acid concentration and temperature. The removal efficiency of acrylic acid at concentration 720 mg L^{-1} was as high as 99 % with CaO_2 nanoparticle dosage 1 g L^{-1} and

Table 5 – Comparisons of the kinetic models adsorption rate constants, initial adsorption rate, and calculated and experimental q_e values obtained at different acrylic acid concentrations

Initial conc. (mg L^{-1})	$q_{e,\text{exp}}$ (mg g^{-1})	Pseudo-first-order kinetic model			Pseudo-second-order kinetic model			
		k_1 (min^{-1})	$q_{e,\text{cal}}$ (mg g^{-1})	R^2	$k_2 \cdot 10^{-4}$ ($\text{mg mg}^{-1} \text{min}^{-1}$)	$q_{e,\text{cal}}$ (mg g^{-1})	h ($\text{mg mg}^{-1} \text{min}^{-1}$)	R^2
2882	2738.28	0.28	2633	0.91	1.96	2753	1487	0.99
4323	3170.64	0.38	2991	0.72	2.14	3080	2031	0.90
5764	3494.91	0.33	3417	0.98	2.94	3526	2085	0.99

contact time 125 minutes. The adsorption of acrylic acid onto CaO₂ nanoparticles follows a pseudo-second-order kinetics, and Redlich-Peterson model was the best-fitted isotherm. The percent desorption of acrylic acid from the surface of CaO₂ nanoparticles was found to be 64.4 %. The results indicated that CaO₂ nanoparticles are a promising and potential candidate for the recovery of acrylic acid from aqueous system.

References

1. *Straathof, A. J. J., Sie, S., Franco, T. T., Van der Wielen, L. A. M.*, Feasibility of acrylic acid production by fermentation, *Appl. Microbiol. Biotechnol.* **67** (2005) 727. doi: <https://doi.org/10.1007/s00253-005-1942-1>
2. *Jones, T., Dunwoodie, M., Boucher-Ferte, V., Reiff, O.*, *Chemicals for Beginners: The Vth Edition*, (2011) 269.
3. *Keshav, A., Chand, S., Wasewar, K. L.*, Reactive extraction of acrylic acid using tri-n-butyl phosphate in different diluents, *J. Chem. Eng. Data* **54** (2009) 1782. doi: <https://doi.org/10.1021/je800856e>
4. *Xiaobo, X., Jianping, L., Peilin, C.*, Advances in the research and development of acrylic acid production from biomass, *Chin. J. Chem. Eng.* **14** (2006) 419. doi: [https://doi.org/10.1016/S1004-9541\(06\)60094-3](https://doi.org/10.1016/S1004-9541(06)60094-3)
5. *Keshav, A., Wasewar, K. L., Chand, S., Uslu, H.*, Effect of binary extractants and modifier–diluents systems on equilibria of propionic acid extraction, *Fluid Phase Equilib.* **275** (2009) 21. doi: <https://doi.org/10.1016/j.fluid.2008.09.012>
6. *Keshav, A., Wasewar, K. L., Chand, S.*, Recovery of propionic acid from an aqueous stream by reactive extraction: effect of diluents, *Desalin.* **244** (2009) 12. doi: <https://doi.org/10.1016/j.desal.2008.04.032>
7. *Choi, J. I., Hong, W. H.*, Recovery of lactic acid by batch distillation with chemical reactions using ion exchange resin, *J. Chem. Eng. of Jpn.* **32** (1999) 184. doi: <https://doi.org/10.1252/jcej.32.184>
8. *Kuila, S. B., Ray, S. K.*, Dehydration of acetic acid by pervaporation using filled IPN membranes, *Sep. Purif. Tech.* **81** (2011) 295. doi: <https://doi.org/10.1016/j.seppur.2011.07.033>
9. *Mahajan, Y. S., Shah, A. K., Kamath, R. S., Salve, N. B., Mahajani, S. M.*, Recovery of trifluoroacetic acid from dilute aqueous solutions by reactive distillation, *Sep. Puri. Tech.* **59** (2008) 58. doi: <https://doi.org/10.1016/j.seppur.2007.05.027>
10. *Dhongde, V., Wasewar, K. L., De, B. S.*, Development of nanohybrid adsorbent for defluoridation from aqueous systems, *Chemosphere* **188** (2017) 354. doi: <https://doi.org/10.1016/j.chemosphere.2017.08.153>
11. *Singh, K., Lataye, D. H., Wasewar, K. L.*, Removal of fluoride from aqueous solution by using bael (*Aegle marmelos*) shell activated carbon: Kinetic, equilibrium and thermodynamic study, *J. Fluor. Chem.* **194** (2017) 23. doi: <https://doi.org/10.1016/j.jfluchem.2016.12.009>
12. *Singh, K., Lataye, D. H., Wasewar, K. L.*, Removal of fluoride from aqueous solution by using low-cost sugarcane bagasse: Kinetic study and equilibrium isotherm analysis, *J. Haz. Tox. Rad. Waste* **3** (2016) 1. doi: [https://doi.org/10.1061/\(ASCE\)JHZ.2153-5515.0000309](https://doi.org/10.1061/(ASCE)JHZ.2153-5515.0000309)
13. *Singh, K., Lataye, D. H., Wasewar, K. L.*, Adsorption of fluoride onto sugarcane bagasse: An application of Taguchi's design of experimental methodology, *J. Ind. Wat. Works Ass.* **1** (2015) 285.
14. *Singh, K., Lataye, D. H., Wasewar, K. L., Yoo, C. K.*, Removal of fluoride from aqueous solution: status and techniques, *Desal. Water Treat.* **51** (2013) 3233. doi: <https://doi.org/10.1080/19443994.2012.749036>
15. *Kumar, P., Rao, R., Chand, S., Kumar, S., Wasewar, K. L., Yoo, C. K.*, Adsorption of lead from aqueous solution onto coir-pith activated carbon, *Desal. Water Treat.* **51** (2013) 2529. doi: <https://doi.org/10.1080/19443994.2012.749009>
16. *Kumar, P., Agnihotri, R., Wasewar, K. L., Uslu, H., Yoo, C. K.*, Status of adsorptive removal of dye from textile industry effluent, *Desal. Water Treat.* **50** (2012) 226. doi: <https://doi.org/10.1080/19443994.2012.719472>
17. *Gulipalli, C. S., Prasad, B., Wasewar, K. L.*, Batch study, equilibrium, kinetics of adsorption of selenium using rice husk ash (RHA), *J. Eng. Sci. Tech.* **6** (2011) 590.
18. *Kumar, P., Chand, S., Padmini, B. N., Teng, T. T., Wasewar, K. L.*, Adsorption of cadmium ions from aqueous solution using granular activated carbon and activated clay, *CLEAN: Soil Air Water* **38** (2010) 49.
19. *Wasewar, K. L.*, Adsorption of metals onto tea factory waste: A review, *Int. J. Res. Rev. App. Sci.* **3** (2010) 303.
20. *Gulipalli, C. S., Prasad, B., Wasewar, K. L.*, Removal of selenium by adsorption onto granular activated carbon (GAC) and powdered activated carbon (PAC), *CLEAN* **37** (2009) 872.
21. *Gulipalli, C. S., Prasad, B., Wasewar, K. L.*, Adsorption of selenium using bagasse fly ash (BFA) *CLEAN* **37** (2009) 534.
22. *Kumar, S., Prasad, B., Wasewar, K. L.*, Adsorption of tin using granular activated carbon, *J. Env. Prot. Sci.* **3** (2009) 41.
23. *Atif, M., Prasad, B., Wasewar, K. L., Mishra, I. M.*, Batch Adsorption of Zn using tea factory waste as an adsorbent, *Desalination* **244** (2009) 66. doi: <https://doi.org/10.1016/j.desal.2008.04.036>
24. *Atif, M., Prasad, B., Wasewar, K. L.*, Characterization of factory tea waste as an adsorbent for removal of heavy metals, *J. Fut. Eng. Tech.* **3** (2008) 47.
25. *Rajoriya, R. K., Prasad, B., Mishra, I. M., Wasewar, K. L.*, Adsorption of benzaldehyde on granular activated carbon: Kinetics, equilibrium, and thermodynamic, *Chem. Biochem. Eng.* **22** (2007) 219.
26. *Wasewar, K. L., Ravichandra, Y., Kumar, A. M., Godbole, V.*, Adsorption mechanism for the adsorption of heavy metals using tea waste as an adsorbent, *J. Future Eng. Tech.* **3** (2006) 41.
27. *Aşçı, Y. S., Hasdemir, I. M.*, Removal of some carboxylic acids from aqueous solutions by hydrogels, *J. Chem. Eng. Data* **53** (2008) 2351. doi: <https://doi.org/10.1021/je800230t>
28. *Uslu, H., İnci, I., Bayazit, S. S.*, Adsorption equilibrium data for acetic acid and glycolic acid onto Amberlite IRA-67, *J. Chem. Eng. Data* **55** (2010) 1295. doi: <https://doi.org/10.1021/je900635z>
29. *Madan, S. S., Wasewar, K. L., Kumar, C. R.*, Adsorption kinetics, thermodynamics, and equilibrium of α -toluic acid onto calcium peroxide nanoparticles, *Ad. Pow. Tech.* **27** (2016) 2112. doi: <https://doi.org/10.1016/j.apt.2016.07.024>

30. Roncaroli, F., Blesa, M. A., Kinetics of adsorption of carboxylic acids onto titanium dioxide, *Phys. Chem. Chem. Phys.* **12** (2010) 9938.
doi: <https://doi.org/10.1039/c003086d>
31. López-Velandia, C., Moreno-Barbosa, J. J., Sierra-Ramirez, R., Giraldo, L., Moreno-Piraján, J. C., Adsorption of volatile carboxylic acids on activated carbon synthesized from watermelon shells, *Adsorpt. Sci. Technol.* **32** (2014) 227.
doi: <https://doi.org/10.1260/0263-6174.32.2-3.227>
32. Tong, S. R., Wu, L. Y., Ge, M. F., Wang, W. G., Pu, Z. F., Heterogeneous chemistry of monocarboxylic acids on α -Al₂O₃ at different relative humidities, *Atmos. Chem. Phys.* **10** (2010) 7561.
doi: <https://doi.org/10.5194/acp-10-7561-2010>
33. Madan, S. S., Wasewar, K. L., Kumar, C. R., Optimization of adsorptive removal of α -toluic acid by CaO₂ nanoparticles using response surface methodology, *Res. Eff. Tech.* **3** (2017) 88.
34. Madan, S. S., Wasewar, K. L., Pandharipande, S. L., Modeling the adsorption of benzenecetic acid on CaO₂ nanoparticles using artificial neural network, *Res. Eff. Tech.* **2** (2016) 53.
doi: <https://doi.org/10.1016/j.reffit.2016.10.004>
35. Madan, S. S., Wasewar, K. L., Pandharipande, S. L., Artificial Neural Network (ANN) method for modeling of benzenecetic acid adsorption using CaO₂ nanoparticles, *Sep. Tech. Chem. Biochem. Petro. Env. Eng.* **10** (2016).
36. Waghmare, M. D., Wasewar, K. L., Sonawane, S. S., Kinetics and thermodynamics of picolinic acid adsorption on low cost adsorbent peanut hull, *Res. J. Chem. Env.* **18** (2014) 87.
37. Hochella, M. F., Madden, A. S., Earth's nano-compartment for toxic metals, *Elements* **1** (2005) 199.
doi: <https://doi.org/10.2113/gselements.1.4.199>
38. Baillieul, H., Moor, G. D., Leys, W., Geert, K. V., Burdick, J., Gevaerts, W., Enhanced bioremediation of a BTEX contaminated soil in Belgium. IXPBR Ca H₂O₂ Remediation Arcadis-236820.pdf.
39. Park, J. W., Park, B. K., Kim, J. E., Remediation of soil contaminated with 2,4-dichlorophenol by treatment of minced shepherd's purse roots, *Arch. Env. Contamin. Tox.* **50** (2006) 191.
doi: <https://doi.org/10.1007/s00244-004-0119-8>
40. Northup, A., Cassidy, D., Calcium peroxide (CaO₂) for use in modified Fenton chemistry, *J. Hazard. Mat.* **152** (2008) 1164.
doi: <https://doi.org/10.1016/j.jhazmat.2007.07.096>
41. Madan, S. S., Upwanshi, W. A., Wasewar, K. L., Adsorption of α -toluic acid by calcium peroxide nanoparticles, *Desalin. Water Treat.* **57** (2016) 16507.
doi: <https://doi.org/10.1080/19443994.2015.1079255>
42. Olyai, E., Banejad, H., Afkhami, A., Rahmani, A., Khodaveisi, J., Development of a cost-effective technique to remove the arsenic contamination from aqueous solutions by calcium peroxide nanoparticles, *Sep. Puri. Tech.* **95** (2012) 10.
43. Andrews, L., Chertihin, G. V., Thompson, C. A., Dillon, J., Byrne, S., Bauschlicher, C. W., Infrared spectra and quantum chemical calculations of group 2 MO₂, O₂MO₂, and related molecules, *The J. Phy. Chem.* **100** (1996) 100.
doi: <https://doi.org/10.1021/jp9519934>
44. Umemura, J., Hayashi, S., Infrared spectra and molecular configurations of liquid and crystalline acrylic acid, *Bull. Inst. Chem. Res., Kyoto Univ.* **52** (1974) 585.
45. Langmuir, I., The constitution and fundamental properties of solids and liquids, *J. The Am. Chem. Soc.* **38** (1916) 2221.
doi: <https://doi.org/10.1021/ja02268a002>
46. Freundlich, U., Die adsorption in lusungen, *J. Phy. Chem.* **57** (1906) 385.
47. Dąbrowski, A., Adsorption from theory to practice, *Adv. Coll. Inter. Sci.* **93** (2001) 135.
doi: [https://doi.org/10.1016/S0001-8686\(00\)00082-8](https://doi.org/10.1016/S0001-8686(00)00082-8)
48. Tempkin, M. I., Pyzhev, V., Kinetics of ammonia synthesis on promoted iron catalyst, *ActaPhys. Chim. USSR* **12** (1940) 327.
49. Hill, A. V., The possible effects of the aggregation of the molecules of haemoglobin on its dissociation curves, *J. Physiol.* **40** (1910) 4.
50. Koopal, L. K., Van, Riemsdijk, W. H., De-Wit, J. C., Benedetti, M. F., Analytical isotherm equations for multicomponent adsorption to heterogeneous surfaces, *J. Coll. Inter. Sci.* **166** (1994) 51.
doi: <https://doi.org/10.1006/jcis.1994.1270>
51. Sips, R., On the structure of a catalyst surface, *The J. Chem. Phy.* **16** (1948) 490.
doi: <https://doi.org/10.1063/1.1746922>
52. Xiong, L., Yang, Y., Mai, J., Sun, W., Zhang, C., Wei, D., Chen, Q., Ni, J., Adsorption behavior of methylene blue onto titanate nanotubes, *C. Eng. J.* **156** (2010) 313.
doi: <https://doi.org/10.1016/j.cej.2009.10.023>